Tracer diffusion of hafnium, niobium and zirconium in Hf-Nb alloys

1995 J. Phys.: Condens. Matter 7 9185

(http://iopscience.iop.org/0953-8984/7/48/009)

J. Phys.: Condens. Matter 7 (1995) 9185–9200. Printed in the UK

Tracer diffusion of hafnium, niobium and zirconium in Hf–Nb alloys

P Knorr and Chr Herzig

Institut für Metallforschung, Universität Münster, Wilhelm-Klemm-Strasse 10, D-48149 Münster, Germany

Received 18 July 1995, in final form 25 September 1995

Abstract. The tracer diffusion of ^{181}Hf, ^{95}Nb and ^{95}Zr was measured in the bcc structure of a Hf–Nb(10 at.%) and a Hf–Nb(18 at.%) alloy. It was the primary aim of the measurements to test whether self-diffusion in the two alloys investigated is in accordance with the Arrhenius law of diffusion or reveals any *curvature*, as was previously found for bcc Zr–Nb alloys of different composition. For Zr–Nb alloys a continuous change in the diffusion anomaly with respect to self-diffusion in pure bcc Zr was found, reflecting the systematic variation in the electronic structure when alloying group V to group VI bcc transition metals. The classification of self-diffusion in bcc hafnium as normal or 'anomalous' has not been possible so far because of the rather limited existence range of its bcc phase of only 485 K. Alloying Hf with the group V metal Nb stabilizes the bcc structure down to lower temperatures and extends its existence range considerably. Since the model of phonon-related diffusion predicts self-diffusion in bcc Hf to show in principle a curved Arrhenius plot, one could expect this curvature to be revealed in the two Hf–Nb alloys. However, the measurements yielded *straight* Arrhenius plots for the Hf–Nb(10 at.%) and the Hf–Nb(18 at.%) alloy. Since the tracer diffusion of the alloying component Nb was studied as well, the random alloy model for concentrated solid solutions allowed the calculation of the partial correlation factors f_{Hf} and f_{Nb}. The values of f extrapolated to pure bcc hafnium are in good agreement with the theoretical value for monovacancy diffusion.

1. Introduction

While the Arrhenius law of diffusion, determined by the pre-exponential factor D_0 and the activation enthalpy Q,

$$D = D_0 \exp\left(-\frac{Q}{kT}\right) \tag{1}$$

is obeyed in most crystalline solids, it is seriously violated in the whole class of bcc metals (see figure 1). All bcc metals with an extended temperature range of the bcc phase except Cr show a distinct nonlinearity in their Arrhenius plots of self-diffusion. (For a compilation of the data see [1].) In the Arrhenius presentation self-diffusion in fcc metals lies well within a narrow band of roughly two orders of magnitude at a temperature $T = T_m/2$, described by $(0.05 \leqslant D_0 \leqslant 5) \times 10^{-4}$ m^2 s^{-1} and $Q = 1.5 \times 10^{-3} T_m$ eV. In contrast, self-diffusion in bcc metals is characterized by an extremely large spreading of the mobility, covering seven orders of magnitude at $T = T_m/2$.

Moreover, self-diffusion in bcc metals is in accordance with a certain systematics: for the bcc transition metals diffusivity increases with increasing d-electron concentration and increases within one group when proceeding to d bands of higher order [2].

0953-8984/95/489185+16$19.50

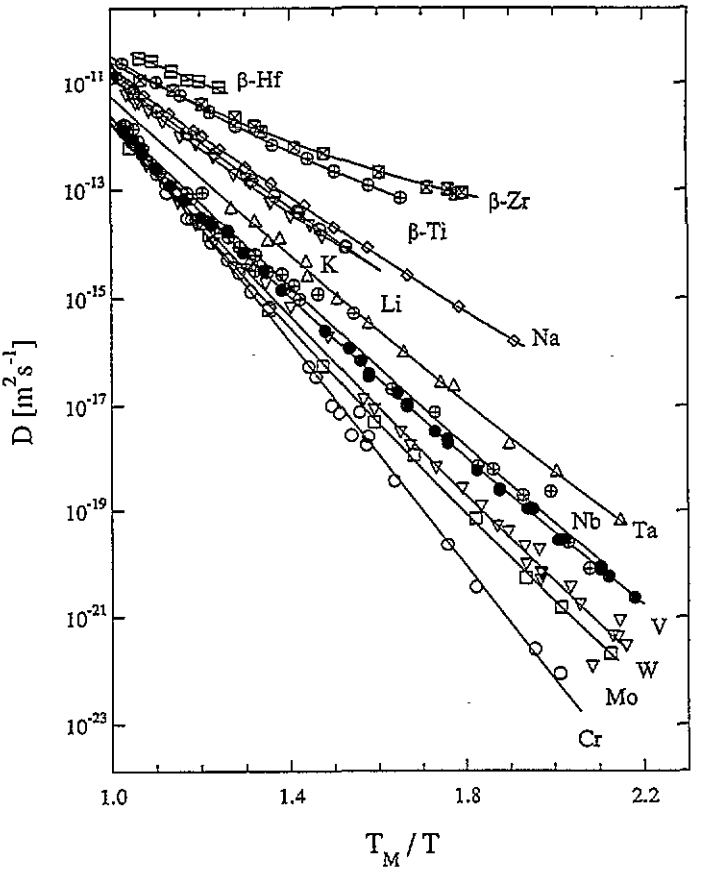

Figure 1. An Arrhenius plot of the self-diffusion in bcc metals on a temperature scale normalized to the melting temperature T_m.

From these three characterizing features of self-diffusion in bcc metals—the broad spectrum of Q and D_0, the curvature of the Arrhenius plots and the systematics—the *curvature* has always been of central interest. Formally two mathematically different treatments have been proposed for the description of a curved Arrhenius plot: either (a) the curvature can be regarded as being due to the sum of several exponentials, each with a different Q^i and D_0^i:

$$D(T) = \sum_i D_0^i \exp\left(-\frac{Q^i}{kT}\right) \tag{2}$$

or (b) the curvature may be created by an explicitly temperature-dependent parameter Q of monovacancy diffusion:

$$D(T) = D_0(T) \exp\left(-\frac{Q(T)}{kT}\right). \tag{3}$$

Generally speaking, the physical content of (a) is that diffusion is regarded to occur via several different mechanisms. Here the curvature has commonly been ascribed to the influence of divacancies [3] or self-interstitials [4] which give rise to an enhanced diffusivity with increasing temperature in addition to a simple monovacancy mechanism. Very recently

the ring mechanism, i.e. the direct interchange of two or more atoms, has been discussed again as a possible diffusion mechanism in certain bcc metals [5].

Explanations according to (b) took into account both a possible temperature dependence of the vacancy formation enthalpy H^f and of the migration enthalpy H^m [6–9]. Since the enthalpies of vacancy formation, H^f, and migration, H^m, which both enter into Q, are related to the pertaining entropies, S^f and S^m, according to the Maxwell relation $(\partial H/\partial T)_p = T(\partial S/\partial T)_p$, the pre-exponential factor D_0 will necessarily be temperature dependent too.

Basically, these considerations were focused on the possible influence of lattice anharmonicity which is generally regarded as being responsible for the (nonlinear) temperature dependence of most macroscopic physical quantities of solids like elastic moduli, thermal expansion coefficients, and bulk moduli. Consistently, former models tried to link the defect enthalpies of diffusion with these temperature-dependent properties.

When during recent years inelastic neutron scattering (INS) experiments on many bcc transition metals and alloys yielded a more detailed understanding of the respective lattice dynamics, the considerations were no longer restricted to the rather crude macroscopic dynamical properties, but could be founded on the subtleties of the phonon dispersion curves [10–14]. In order to make use of this large pool of data Schober *et al* [15] developed a model that allowed a direct calculation of the migration enthalpy H^m from the phonon density of states. Since for many bcc transition metals the latter turned out to be significantly temperature dependent, temperature-dependent vacancy migration enthalpies were obtained.

While because there are several serious objections the *multidefect* point of view (a) has been abandoned for bcc metals [8, 16], the interpretation (b) in which temperature-dependent defect enthalpies account for the curved Arrhenius plots is still under discussion. It is the aim of this paper to test interpretation (b) experimentally. So far T-dependent migration enthalpies have been calculated for β-Zr, Nb, Mo and Cr on the basis of phonon dispersion measurements [15]. Except for Cr, these metals reveal curved Arrhenius plots for self-diffusion [17–21]. Yet a survey of the available self-diffusion data for bcc metals (see figure 1) leaves the question open of whether the group IV transition metal β-Hf reveals a curved Arrhenius plot too. As the bcc structure of Hf exists over the rather limited range between 2015 K and 2500 K only, it is likely that the probable curvature was concealed by the scatter of the measured diffusion coefficients at such high temperatures [22]. On first looking at the dynamical properties of β-Hf one can reasonably assume the Arrhenius plot to be nonlinear: the phonon dispersion of β-Hf very much resembles that of the chemically related elements β-Ti and β-Zr [10–12]. These two group IV transition metals reveal the most distinct curvature in the Arrhenius diagram (see figure 1) [23, 17] and both show a strong T-dependence of the soft T_1 (110) phonon branch which was regarded as having a particular influence on the migration enthalpy H^m [9].

In order to improve the experimental conditions for detecting the model-predicted curvature in the bcc phase of Hf from self-diffusion measurements, the range of existence of the bcc phase of Hf was extended considerably in the present investigation by alloying Hf with Nb. According to the equilibrium phase diagram [24], β-Hf and Nb form a complete solid solution at high temperatures. Alloying Hf with, e.g., 10 at.% Nb up to the eutectoid composition of 18 at.% Nb stabilizes the bcc structure down to 1630 K and 1090 K, respectively, thereby extending its range of existence over 780 K and 1300 K. The expectation that the curvature could be revealed in these alloys was supported by previous measurements on the influence of group V and group VI elements on the self-diffusion behaviour of group IV metals: it was shown that although alloying of, for example, Nb to β-Zr [2] or Mo to β-Ti [25] normalizes the self-diffusion behaviour, i.e. the degree of

curvature of the Arrhenius plots is diminished, a curvature nevertheless remains clearly visible. This is shown in figure 2, left panel. Up to a Nb concentration of 28.1 at.% the Arrhenius plot of Zr self-diffusion in the Zr–Nb alloys has still not become entirely linear.

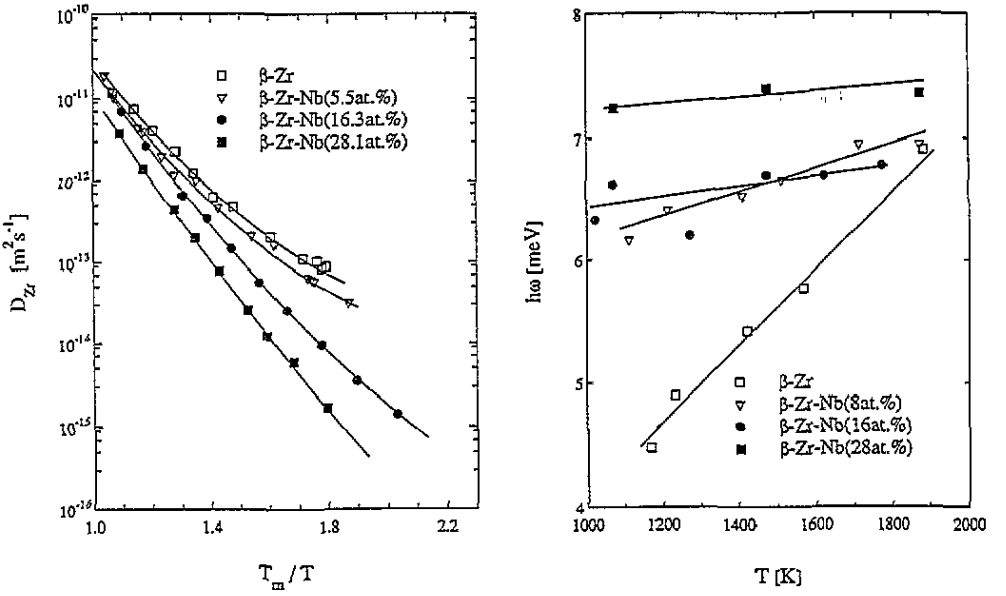

Figure 2. The left-hand panel shows the temperature dependence of ^{95}Zr diffusion in the bcc phase of Zr [17] and of Zr–Nb alloys [2], plotted in Arrhenius form on a normalized temperature scale, while the right-hand panel shows the temperature dependence of the zone-boundary phonon ($\xi = 0.5$) in the T_1 ($\xi\xi 0$) phonon branch for β-Zr and β-Zr–Nb alloys [33].

When investigating Hf self-diffusion in a binary Hf–Nb alloy it is particularly meaningful to measure the diffusion of the alloying component Nb as well. With both tracer diffusion coefficients known, the random alloy model developed by Manning for concentrated solutions [26, 27] allows the calculation of the partial correlation factors f_{Hf} and f_{Nb}.

2. Experimental details

Hf–Nb alloys of two compositions were produced, one having a Nb content of 10 at.% and the other one having a content of 18 at.% (eutectoid composition). Hf (principal impurities (wt ppm): Zr, 129; Ta, <100; Nb, <50; Fe, <50; Zn, <50) was supplied by Wah Chang Albany, while Nb (principal impurities (wt ppm): Ta, 880; O, 75; Al, <50; Si, <50) was provided by Companhia Brasileira de Metalurgia e Mineracao. The Hf–Nb(18 at.%) alloy was melted in an electron beam furnace in a vacuum of 10^{-4} Pa while the Hf–Nb(10 at.%) alloy was prepared by arc melting in an oxygen-purified 5N Ar atmosphere. The homogeneity and absolute concentration of both alloys were repeatedly checked by electron microprobe analysis yielding a standard deviation of less than 0.4 at.% in absolute concentration. From the alloy ingot, samples 11 mm in diameter were cut by spark erosion. The samples were cleaned of Cu contamination of the spark erosion electrode by strong etching with an acid solution of 40% HNO_3, 40% H_2O and 20% HF. The diameter was reduced to 10 mm with a lathe. After the samples had been polished optically flat with diamond paste they were annealed in a UHV chamber ($p \leqslant 10^{-5}$ Pa) for four hours at

1900 K. This pre-anneal resulted in samples being strongly recrystallized, and consisting of two or three grains only. Optical metallography revealed a fine lamellar eutectoid structure inside the grains due to the decomposition transformation. For the following diffusion anneals the annealing time was chosen in such a way that during the α–β phase transition less than one per cent of the total annealing time was necessary to dissolve the lamellae (width $\leqslant 10$ μm) of the eutectoid to a homogeneous solid solution, allowed by the high diffusivity in the bcc phase.

A mixture of the two radioisotopes ^{175}Hf and ^{181}Hf in a $HfCl_4$ solution was applied. ^{175}Hf has a dominant decay energy of 343 keV, while ^{181}Hf reveals the most intense nuclear decays at energies of 133 keV and 482 keV. The two radioisotopes ^{175}Hf and ^{181}Hf have half-lives of 70 d and 42.4 d, respectively. The nuclide ^{95}Zr was obtained from neutron activation of 90%-enriched ^{94}Zr. Within a β^- transition, ^{95}Zr decays into the radioisotope ^{95}Nb. The characteristic energies of the nuclear transitions are 724 keV and 757 keV for ^{95}Zr and 766 keV for ^{95}Nb. The half-lives of the two radioisotopes are 64 d and 35 d for ^{95}Zr and for ^{95}Nb, respectively. The activated ^{94}Zr was dissolved in a few microlitres of concentrated HF and diluted with twice-distilled water. Both mixtures of radiotracer were dropped onto the surface of the sample and dried under an infrared lamp.

All diffusion anneals were performed under high-vacuum conditions ($p = 10^{-5}$ Pa). For temperatures above 1600 K a special electron heating device was used [17] which—considering the rather short annealing times—allowed a rapid heating up and cooling down of the specimen. For all short-time anneals the annealing time was corrected according to a routine of Itayama and Stüwe [28]. During this heating procedure the diffusion samples were placed inside a closed Nb container. The temperature was measured both with a differential pyrometer and with an optical pyrometer which had been calibrated against a tungsten strip lamp. The total uncertainty in the temperature measurement was estimated to be about ± 10 K.

Diffusion anneals below 1600 K were carried out in a tantalum furnace and the usual resistance-heated tube furnace. Here the temperature was determined with a Pt–PtRh and a Ni–NiCr thermocouple, respectively, with an estimated uncertainty of ± 3 K.

After the diffusion anneals the samples were reduced in diameter with a lathe for $12\sqrt{Dt}$ in order to exclude radial indiffusion. The samples were microsectioned using a lathe for the experiments with large-penetration profiles and a microtome for all others. The slices were weighed with a microbalance in order to determine their thickness accurately from the weight, the diameter and the density of the material. The latter was measured with a hydrostatic balance, determining the hydrostatic buoyancy of the samples in different liquids. The densities are 12.47 g cm^{-3} for Hf–Nb(18 at.%) and 12.82 g cm^{-3} for Hf–Nb(10 at.%).

The decay rates of the ^{181}Hf, ^{95}Zr and ^{95}Nb isotopes in the individual sections were detected by γ-spectroscopy in a well-type intrinsic Ge detector combined with a 4k multi-channel analyser, which achieves the high-energy resolution required for separating the 757 keV decays of ^{95}Zr from the 766 keV decay of ^{95}Nb. Background, half-life, Compton and mother–daughter corrections were performed for all the experiments. With respect to the latter some remarks might be necessary: the mathematical correction for separating the mixture of the mother isotope ^{95}Zr and the daughter isotope ^{95}Nb merely takes into account the additional ^{95}Nb activity that was added to the original ^{95}Nb by the decay of ^{95}Zr *after* the diffusion anneal had been finished, whereas no correction can be applied for those atoms that have migrated as ^{95}Zr, have decayed into ^{95}Nb and continued migrating as ^{95}Nb *during* the anneal. For short annealing times this amount of ^{95}Nb activity can be neglected.

Formally the mother–daughter correction is expressed by

$$c_2 N_2^t(t=0) = \left(N_2^m(t) - \frac{c_2}{c_1} \chi N_1^m(t) \exp(\lambda_1 t) \right) \exp(\lambda_2 t) \tag{4}$$

$$\chi = \frac{\lambda_1}{\lambda_2 - \lambda_1} \left(\exp(-\lambda_1 t) - \exp(-\lambda_2 t) \right). \tag{5}$$

Here the index $i = 1$ refers to the mother nuclide and the index $i = 2$ refers to the daughter nuclide. $N_i^m(t)$ is the measured activity of nuclide i at time t, $N_i^t(t)$is the true activity of nuclide i at time t, λ_i is the decay constant of nuclide i, $c_i = N_i^m(t)/N_i^t(t)$ is the detection efficiency of activity of nuclide i, and $t = 0$ indicates the end of the diffusion anneal.

Since the two isotopes have approximately the same decay energies, their detection efficiencies can be assumed to be equal and c_1/c_2 is approximately unity.

We did not separate the ^{95}Nb radiotracer from the mother isotope ^{95}Zr because simultaneous diffusion of ^{175}Hf, ^{181}Hf, ^{95}Zr and ^{95}Nb not only provides directly comparable results for the application of the random alloy model to the diffusion coefficients obtained, but also yields information about the dependence of diffusion on the atomic radii and on the number of valence electrons. In order to ensure that the simultaneous indiffusion of several radioisotopes does not cause interference between them, some of the experiments were performed for comparison with ^{175}Hf/^{181}Hf radiotracer only.

The measured diffusion profiles were evaluated according to the thin-layer solution of Fick's second equation:

$$c(x,t) = \frac{M}{\sqrt{\pi D t}} \exp\left(-\frac{x^2}{4Dt} \right) \tag{6}$$

with the relative specific tracer concentration c, the depth coordinate x, the annealing time t, the tracer diffusion coefficient D and the tracer concentration M per unit area at $x = 0$ and $t = 0$.

Table 1. Results fot the self-diffusion of ^{181}Hf, ^{95}Zr and ^{95}Nb in β-Hf–Nb(18 at.%).

T (K)	t (s)	D_{Hf} (m^2 s^{-1})	D_{Zr} (m^2 s^{-1})	D_{Nb} (m^2 s^{-1})
1257	171 900	1.57×10^{-15}	2.38×10^{-15}	7.97×10^{-16}
1276	175 620	1.55×10^{-15}		
1319	171 540	5.19×10^{-15}	7.00×10^{-15}	3.18×10^{-15}
1388	88 320	1.28×10^{-14}		
1529	27 000	1.20×10^{-13}	1.76×10^{-13}	6.62×10^{-14}
1633	1980	1.71×10^{-13}	2.40×10^{-13}	1.04×10^{-13}
1785	1800	9.91×10^{-13}		
1853	5460	1.56×10^{-12}		
1981	2070	3.54×10^{-12}	4.96×10^{-12}	3.05×10^{-12}
2051	3240	4.86×10^{-12}		
2173	1620	1.35×10^{-11}	1.85×10^{-11}	1.33×10^{-11}

3. Results

Figures 3 and figure 4 show the penetration profiles of the ^{175}Hf/^{181}Hf diffusion in Hf–Nb(18 at.%) and Hf–Nb(10 at.%), respectively. While all high-temperature profiles show

a perfectly linear decrease of the tracer activity by more than three decades, two of the penetration profiles, which were obtained from experiments at temperatures of 1257 K and 1319 K, exhibit a slight upward curvature in the region close to the surface of the sample. This may result from the formation of hafnium oxides delaying the diffusion from the surface into the bulk. For this reason the respective diffusion coefficients were checked again under even better high-vacuum conditions in a different UHV chamber at comparable temperatures (1276 K and 1388 K). The undisturbed profiles obtained yielded diffusion coefficients in fairly good agreement with the former ones. The diffusion coefficients obtained for the $^{175}Hf/^{181}Hf$ diffusion in Hf–Nb(18 at.%) and Hf–Nb(10 at.%) are summarized in tables 1 and 2, respectively. The total error of each individual diffusion coefficient is approximately 8%, mainly due to the uncertainty in the temperature measurement. In figure 5 the temperature dependences of the Hf diffusion in Hf–Nb(18 at.%) and Hf–Nb(10 at.%) are plotted in Arrhenius form. For comparison self-diffusion in pure β-Hf is shown as well [22]. The calculated pre-exponential factors D_0 and activation enthalpies Q are listed in table 3.

Table 2. Results for the self-diffusion of ^{181}Hf, ^{95}Zr and ^{95}Nb in β-Hf–Nb(10 at.%)

T (K)	t (s)	D_{Hf} ($m^2\ s^{-1}$)	D_{Zr} ($m^2\ s^{-1}$)	D_{Nb} ($m^2\ s^{-1}$)
1758	5400	9.36×10^{-13}	1.16×10^{-12}	8.22×10^{-13}
1863	4860	2.16×10^{-12}	2.96×10^{-12}	1.59×10^{-12}
2003	3600	4.63×10^{-12}		
2113	1860	8.68×10^{-12}	1.14×10^{-11}	7.53×10^{-12}
2268	1800	1.78×10^{-11}	2.42×10^{-11}	1.79×10^{-11}

Table 3. The pre-exponential factor D_0 and activation enthalpy Q of Hf, Zr and Nb diffusion in β-Hf–Nb(10 at.%) and β-Hf–Nb(18 at.%) from the analysis of the Arrhenius plots in figures 4 and 6.

	β-Hf–Nb(18 at.%)		β-Hf–Nb(10 at.%)	
	D_0 ($m^2\ s^{-1}$)	Q (kJ mol^{-1})	D_0 ($m^2\ s^{-1}$)	Q (kJ mol^{-1})
Hf	2.23×10^{-6}	219.4 ± 3.5	4.15×10^{-7}	189.5 ± 3.9
Zr	3.07×10^{-6}	219.3 ± 4.2	6.97×10^{-7}	193.3 ± 8.1
Nb	4.82×10^{-6}	234.7 ± 7.9	7.26×10^{-7}	200.9 ± 5.9

The simultaneously measured penetration profiles of ^{95}Zr and ^{95}Nb tracer diffusion have practically the same shape as those of $^{175}Hf/^{181}Hf$ diffusion. Figures 6 and 7 show some penetration plots of the ^{95}Zr and ^{95}Nb diffusion, respectively, for the Hf–Nb(10 at.%) alloy. The respective diffusion coefficients are listed in table 2. The temperature dependencies of both diffusants are shown in figures 8 and 9 in comparison with the self-diffusion in Hf–Nb(18 at.%) and Hf–Nb(10 at.%). The corresponding diffusion coefficients are given in tables 1 and 2, while the values of the pre-exponential factor D_0 and of the activation enthalpy Q, which were obtained from least-squares fits of the pertaining Arrhenius plots, figures 8 and 9, are summarized in table 3. The systematic deviation from the Arrhenius line of all three sets of tracer diffusion data at 1529 K indicates a nontypical error in the temperature determination of this experiment.

The random alloy model of Manning [26, 27] allows the calculation of the partial correlation factors f_{Hf} and f_{Nb} for the component diffusion coefficients in the case of

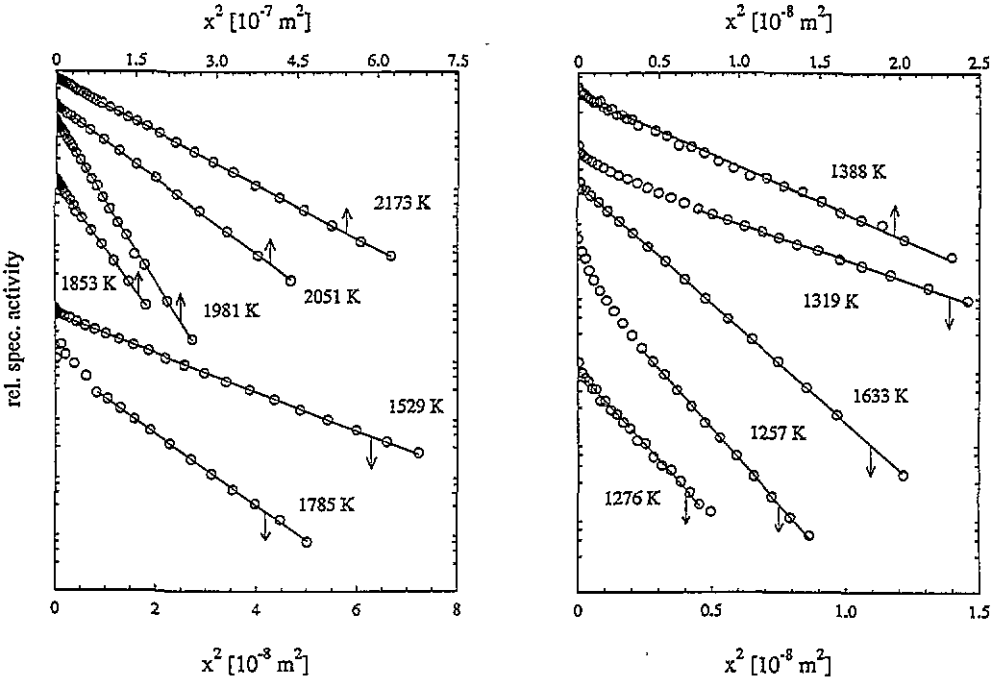

Figure 3. Penetration profiles of ^{181}Hf diffusion in the bcc phase of the Hf–Nb(18 at.%) alloy for higher (left) and lower (right) temperatures.

Table 4. Partial correlation factors f_{Hf} and f_{Nb} of the ^{181}Hf and ^{95}Nb diffusion in β-Hf–Nb(10 at.%) and β-Hf–Nb(18 at.%) according to equations (7) and (8). The last column gives the extrapolated correlation factor f_{Hf} for self-diffusion in pure β-Hf.

	f_{Hf}	f_{Nb}	f_{Hf}	f_{Nb}	f_{Hf}
T (K)	β-Hf–Nb(10 at.%)		β-Hf–Nb(18 at.%)		β-Hf
2100	0.725	0.749	0.722	0.750	0.728
2000	0.724	0.757	0.720	0.759	0.729
1900	0.723	0.765	0.718	0.770	0.729
1800	0.722	0.773	0.716	0.779	0.730
1700	0.721	0.782	0.713	0.790	0.731
1600			0.711	0.802	
1500			0.708	0.815	
1400			0.705	0.829	
1300			0.702	0.843	

vacancy diffusion in binary concentrated alloys:

$$f_{Hf} = \frac{(M_0+2)(N_{Hf}D^*_{Hf} + N_{Nb}D^*_{Nb}) - 2D^*_{Hf}}{(M_0+2)(N_{Hf}D^*_{Hf} + N_{Nb}D^*_{Nb})} \tag{7}$$

$$f_{Nb} = \frac{(M_0+2)(N_{Hf}D^*_{Hf} + N_{Nb}D^*_{Nb}) - 2D^*_{Nb}}{(M_0+2)(N_{Hf}D^*_{Hf} + N_{Nb}D^*_{Nb})}. \tag{8}$$

f_{Hf} and f_{Nb} were calculated from the dependence on temperature of the measured tracer diffusion coefficients D^*_{Hf} and D^*_{Nb} for both alloys investigated, using the Arrhenius

parameters of table 3. In equations (7) and (8) N is the mole fraction and M_0 is a constant which depends on the lattice structure. For the bcc lattice its value is 5.33. The results are listed in table 4. In the temperature range where both alloys exist the partial correlation factors f_{Hf} for the Hf component of Hf–Nb(18 at.%) and Hf–Nb(10 at.%) could be extrapolated to a Nb content of 0 at.%, i.e. to the correlation factor for the self-diffusion in pure β-Hf. The extrapolated values are in close agreement with the theoretically predicted value $f = 0.727$ for monovacancy diffusion.

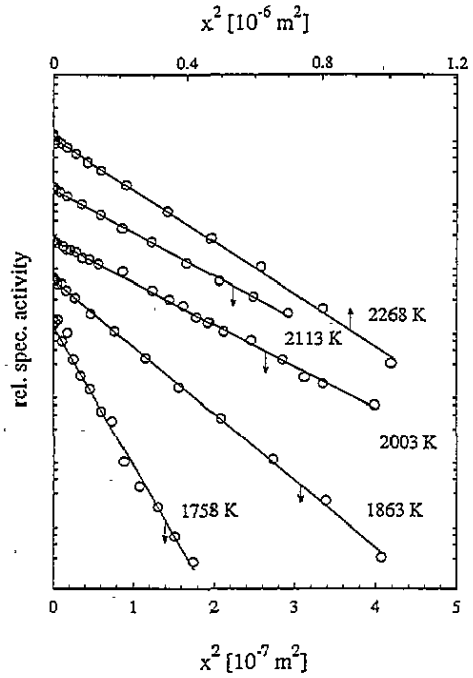

Figure 4. The temperature dependence of ^{181}Hf diffusion in the bcc phase of Hf–Nb(10 at.%), Hf–Nb(18 at.%) and in pure bcc Hf [22] for comparison.

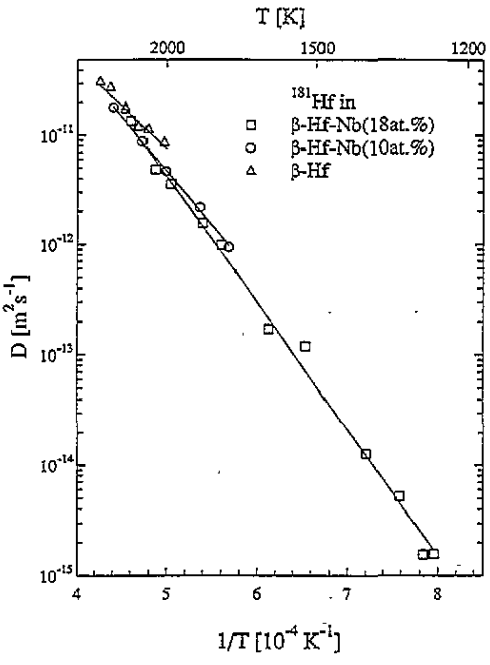

Figure 5. Penetration profiles of ^{181}Hf diffusion in the bcc phase of the Hf–Nb(10 at.%) alloy.

4. Discussion

As is shown in figures 8 and 9, the diffusivities of the three metals, Hf, Zr and Nb, differ only a little from each other. This result is not too surprising considering the position of the three elements in the periodic table and the similarity of their atomic radii. As the diffusivity of the three diffusants is practically the same, one can conclude that the diffusant-atom–vacancy interaction is generally weak and hence the diffusion is obviously controlled by the matrix. Similar results have been obtained by Mundy *et al* for the diffusion of Zr, Nb and W in Nb–W alloys [29]. Investigations by Herzig and Köhler also show only slight differences between the simultaneously diffused elements Zr and Sc in concentrated Zr–Sc [30] and Zr and Nb in concentrated Zr–Nb alloys [2].

The random alloy model for concentrated binary alloys has been developed under the condition that there are no binding energies between the vacancy and the atoms of the

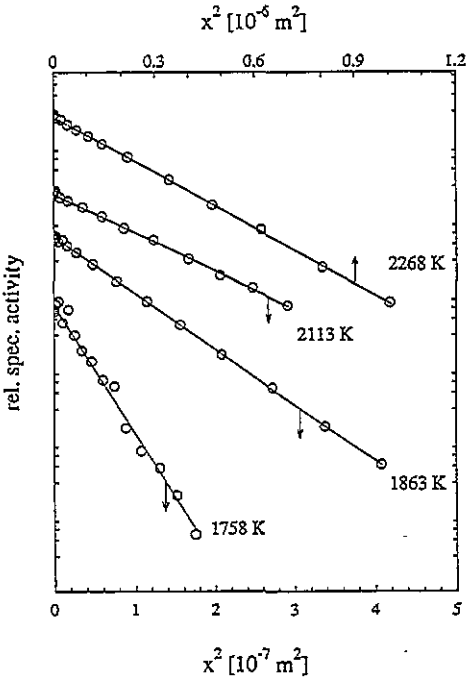

Figure 6. Penetration profiles of ^{95}Zr diffusion in the bcc phase of the Hf–Nb(10 at.%) alloy.

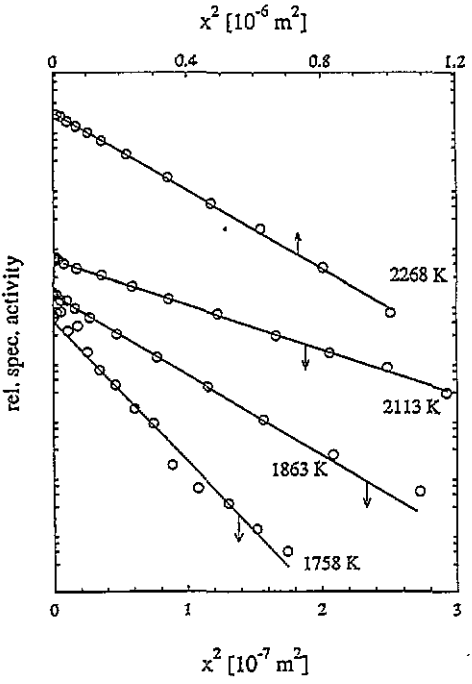

Figure 7. Penetration profiles of ^{95}Nb diffusion in the bcc phase of the Hf–Nb(10 at.%) alloy.

constituents [26, 27]. Furthermore, the model is valid under the assumption that A and B atoms are statistically distributed. The latter assumption is likely to be fulfilled in the system investigated, since Hf and Nb form a solid solution over the whole range of composition in the bcc phase, whereas the first requirement is fulfilled at least to a good approximation because the diffusivities of the three species do not seriously differ from each other.

Table 4 shows that the values of the calculated correlation factors are in the range between 0.702 and 0.725 for f_{Hf} and 0.749 and 0.843 for f_{Nb}. While f_{Hf} remains nearly independent of temperature, f_{Nb} increases continuously to lower temperatures. The reason for this behaviour is the stronger decrease of D_{Nb} with T which enhances the denominator in equation (8). An extrapolation of f_{Hf} to the correlation factor of Hf diffusion in pure β-Hf, f_0, yields values between 0.728 and 0.731 for all temperatures and is thus in good conformity with the theoretical value for the monovacancy mechanism. This finding agrees with the observation provided by quasi-elastic neutron scattering (QNS) experiments in β-Ti [16] that in the temperature range investigated, between 1373 K and 1873 K, diffusion almost exclusively occurs via atomic jumps into NN vacancies .

However, the surprising result of our diffusion measurements is the obvious lack of any curvature of the Hf and Nb diffusion in the Hf–Nb(10 at.%) alloy and especially in the Hf–Nb(18 at.%) alloy, where the temperature range investigated for the bcc phase is certainly sufficiently extended to reveal such an effect.

The assumption that temperature-dependent defect enthalpies are responsible for the observed curvature of self-diffusion in bcc metals was introduced in a model proposed by Köhler and Herzig [8] which gives a qualitative link between dynamical and diffusion

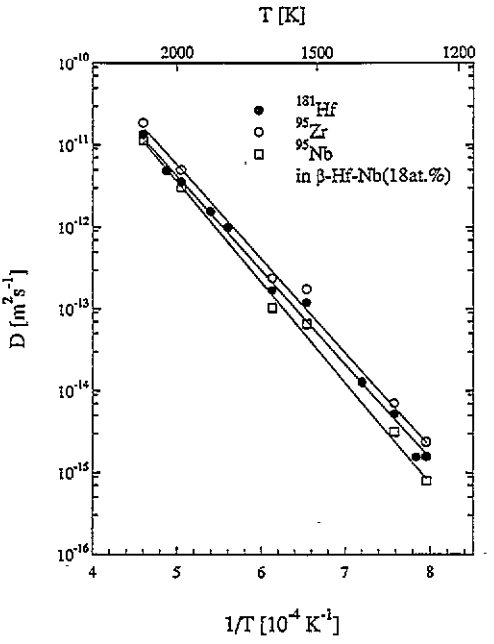

Figure 8. The temperature dependence of ^{181}Hf, ^{95}Zr and ^{95}Nb diffusion in the bcc phase of the Hf–Nb(18 at.%) alloy.

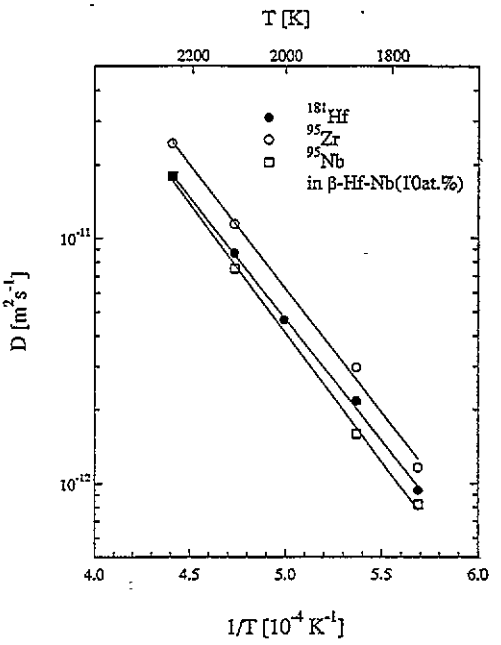

Figure 9. The temperature dependence of ^{181}Hf, ^{175}Hf, ^{95}Zr and ^{95}Nb diffusion in the bcc phase of the Hf–Nb(10 at.%) alloy.

properties. The essence of this model is that the large variation of activation enthalpies of self-diffusion in bcc metals is manifested in the different degrees of softening of the particular low-energy L $\frac{2}{3}(111)$ phonon that in reciprocal space corresponds to the jump vector of a diffusion jump into a NN vacancy. According to this model, the frequency of this jump vector phonon can be regarded as a measure for the height of the migration barrier. Taking into account the curvature of most Arrhenius plots of bcc metals a temperature-dependent migration enthalpy was assumed and, consistently, temperature-dependent phonon frequencies were predicted.

Since extensive experimental data on the phonon dispersion of bcc transition metals has become available in recent years [10–14], one reasonably had to improve on this simple picture and develop a model which took the whole phonon dispersion, instead of only one particular phonon frequency, quantitatively into account. An attempt was made by Schober *et al* [15] whose model has proved to be a powerful tool for the calculation of the migration enthalpy H^m, yielding an excellent agreement between calculated and measured values of H^m for fcc metals. The *temperature behaviour* of the phonon dispersions of several bcc transition metals was recently measured for the first time [10–14]. For some of these metals, especially for β-Zr and Cr, particular phonon branches turned out to shift significantly with temperature. Calculations of H^m using the model of Schober *et al* [15] yielded temperature-dependent migration enthalpies for some of these metals (see table 5).

Due to the considerable experimental difficulties the whole phonon dispersion curve of β-Hf was only measured for one single temperature (2073 K) [12]. The migration enthalpy H^m could therefore be calculated only for that temperature [15], so no information about the temperature behaviour of H^m is available for this metal. It is very likely, however,

Table 5. T_1 $\frac{1}{2}(110)$ phonon frequencies [10, 14] and calculated vacancy migration enthalpies H^m [15].

Material	T (K)	$\hbar\omega$ (meV)	H^m (eV)
β-Ti	1238	7.84	0.31 (1293)
β-Ti	1538	8.16	0.30 (1583)
β-Ti	1713	9.02	0.30 (1783)
β-Zr	1168	4.48	0.28 (1188)
β-Zr	1423	5.42	0.32 (1483)
β-Zr	1883	6.91	0.37
β-Hf	2073	3.34	0.39
β-Hf	2223	4.80	
β-Hf	2293	5.56	
Nb	293	16.2	0.59
Nb	773	15.5	0.62
Nb	1773	14.0	0.62
Nb	2223	13.0	0.58
Cr	293	31.0	0.84 (298)
Cr	673	29.0	0.85
Cr	1073	26.5	0.77
Cr	1473	23.6	0.69
Cr	1773	20.3	0.59

that the migration enthalpy for β-Hf should indeed turn out to be strongly temperature dependent, for the following reasons. It was shown in previous papers [9, 13] that the temperature behaviour of the vacancy migration enthalpy could already be predicted by the behaviour of particular low-energy phonons. In particular, the temperature behaviour of the T_1 $\frac{1}{2}(110)$ zone-boundary phonon can be regarded as a fingerprint for the change of H^m with temperature. This is illustrated in table 5 for several bcc transition metals. A comparison of the T_1 $\frac{1}{2}(110)$ phonon frequencies with the migration enthalpies, calculated using Schober's model, shows that H^m roughly scales with $\omega_{0.5}$: the most pronounced frequency shifts are found for β-Zr and Cr: 54% and 35%, respectively, in the temperature range considered. This finding is reflected in the largest temperature change of H^m (32% and 30%, respectively). For β-Ti [10] and Nb [14] the observed frequency shift of the T_1 $\frac{1}{2}(110)$ phonon is smaller (15% and 19%). This fact consequently yields a very moderate temperature dependence of the calculated migration enthalpies (3% and 7%, respectively) [15].

As mentioned above, the whole phonon dispersion of β-Hf is known for 2073 K only. Part of the dispersion, i.e. the transversal T_1 (110) branch, was measured for 2223 K and 2293 K, too [12]. These measurements actually reveal the most pronounced frequency shift (67%) (see table 5) of all of the group IV to VI bcc transition for metals for which phonon dispersion curves have been measured for various temperatures. Therefore by far the largest change of H^m with temperature is to be expected. According to the models [8, 9] described above, we expected this temperature dependence of H^m of pure β-Hf to be mirrored by curved Arrhenius plots of self-diffusion in the two Hf–Nb alloys investigated. As the present experiments do not reveal any curvature, we will indicate in the following the possible reason(s) for this obvious conflict between theoretical expectation and experimental results.

(i) There is, after all, still no definite proof for a temperature-dependent vacancy migration enthalpy H^m in pure β-Hf. What has been pointed out above is an argumentation on the basis of parts of the dispersion only.

(ii) The limits of uncertainty of the measured Arrhenius relation for self-diffusion in β-Hf–Nb(18 at.%) (see figure 5) are not small enough to exclude the possibility of there being *some* curvature. However, they are definitely small enough to rule out a degree of curvature comparable to those which were found for self-diffusion in β-Zr–Nb alloys (see figure 2, left panel). When a three-parameter fit according to $\ln D = a_0 + a_1\beta + a_2\beta^2$ with $\beta = 1/kT$ is applied to the Arrhenius relations shown in figure 2, left panel, curvature parameters a_2 of 0.13 eV^2 for pure Zr, 0.12 eV^2 for Zr–Nb(5.5 at.%), 0.07 eV^2 for Zr–Nb(16 at.%) and 0.05 eV^2 for Zr–Nb(28 at.%) are obtained. Applying a three-parameter fit to the alloy β-Hf–Nb(18 at.%) currently being investigated yields a downward curvature, i.e. $a_2 < 0$. The reason for this is the deviation of the diffusion coefficients at 1276 K and 1529 K from the Arrhenius line. When the two respective sets of diffusion data are neglected, the remaining data permit one to introduce a curvature parameter $a_2 = 0.02$ eV^2, i.e. for $a_2 > 0.02$ eV^2 the standard deviation of the three-parameter fit becomes larger than that of the straight-line fit.

(iii) A possible objection against our expectation is that the systematics of alloying effects on self-diffusion behaviour in Zr–Nb alloys cannot be reasonably transferred to the Hf–Nb system.

Actually, the obvious difference between β-Hf and its isoelectronic neighbours β-Ti and β-Zr is the considerably smaller temperature range of stability of the bcc structure: while the bcc structure exists within a range of 777 K in β-Ti and 990 K in β-Zr it covers only 485 K for β-Hf, already indicating the larger structural instability. It was shown [32] that the β–α phase transition of group IV elements is actually *phonon controlled* in a way in which particular phonons, which give rise to lattice displacements into the hcp-like structure, are softened when the temperature decreases and approaches the β–α phase transition temperature. $T_{\beta\alpha}$ is then roughly determined by that temperature at which the T_1 $\frac{1}{2}(110)$ phonon particularly involved reaches its critical amplitude—sufficiently large to initiate the β–α transition. For the group IV metals it was found that the softening of this T_1 $\frac{1}{2}(110)$ phonon is considerably larger for β-Hf than for β-Ti and β-Zr (see table 5), hereby reflecting the particularly small range of existence of the bcc structure of hafnium.

Alloying a group V metal to a group IV metal stabilizes the bcc structure to lower temperatures. This correspondingly means for the β–α transition driving the T_1 $\frac{1}{2}(110)$ phonon that its softening, i.e. $\partial\nu_{0.5}/\partial T$, is diminished. Therefore the critical amplitude is achieved at lower temperatures as well. The softening of the T_1 $\frac{1}{2}(110)$ mode successively decreases in Zr–Nb alloys with increasing Nb content (see figure 2, right-hand panel) [33], which was clearly verified by experiment. For Zr–Nb alloys the decrease of softening of the respective phonons is accompanied by a decrease in curvature or *normalization* of the Arrhenius plots of self-diffusion, which has been shown for Zr–Nb alloys with Nb contents of 5.5, 16.3 and 28.1 at.% (see figure 2, left panel). A comparison of the phase diagrams of the Zr–Nb and the Hf–Nb system [24], however, reveals that the above-outlined stabilization effect of the bcc phase upon alloying is much larger for the Hf–Nb than for the Zr–Nb system: for the Zr–Nb(16.3 at.%) alloy the range of existence of the bcc structure is extended by a factor of 1.06, while this remains nearly constant for the Zr–Nb(5.5 at.%) and the Zr–Nb(28.1 at.%) alloy, due to the simultaneous decrease of the phase transition temperature and the melting temperature. In contrast to this moderate stabilization effect, the bcc structures of Hf–Nb(10 at.%) and of Hf–Nb(18 at.%) are enormously extended in their temperature range, by factors of 1.61 and 2.70, respectively. Because of this drastic

stabilization of the high-temperature phase it might be argued that the pronounced phonon softening in pure β-Hf (see table 5) decreases much more rapidly with increasing Nb content than in the Zr–Nb alloys of comparable concentration. In this case the observed and outlined correspondence between phonon softening and curvature of the pertaining Arrhenius relations in Zr–Nb alloys leads to the conclusion that the normalization effect on the possibly curved Arrhenius relation for self-diffusion in pure β-Hf is too strong to reveal any curvature in the Arrhenius plots of the Hf–Nb alloys investigated.

A strong normalization of the Arrhenius relation was also observed for ^{44}Ti diffusion in Ti–Cr(8.4 at.%) and Ti–Mo(9.8 at.%) alloys as compared to the situation in pure β-Ti [25]. In these group IV–VI alloys the bcc structure is stabilized similarly to in the Zr–Nb alloys. However, the d-electron concentration is increased to a larger extent than in the group IV–V alloys. According to the outlined group systematics a smaller phonon softening is expected, which was indeed observed experimentally [33].

In the isoelectronic, equiatomic Ti–Zr(50 at.%) alloy, on the other hand, ^{44}Ti and ^{95}Zr diffusion reveal roughly the same curvature in their Arrhenius relations [34] as self-diffusion in pure β-Ti and β-Zr. In the Ti–Zr system the range of existence of the bcc phase changes only little upon alloying.

(iv) The observed inconsistency between experimental results and the underlying model of phonon-related diffusion requires us to check whether the observed discrepancy is exceptional or whether there are more conflicting results which cannot satisfactorily be explained by the proposed models. It is, for example, not fully clear why for the above-mentioned Zr–Nb(28.1 at.%) alloy a curved Arrhenius plot is still observable [2] although the respective phonons are already almost independent of temperature (see figure 2) [33]. Furthermore, for β-Ti the vacancy migration enthalpy H^m, as obtained from Schober's calculations (see [33]), hardly reveals any temperature dependence (see table 5). Yet, the Arrhenius relation for self-diffusion exhibits a considerable nonlinearity [23]. Also an example of the opposite case can be given: it can hardly be understood why Cr is the only bcc metal showing a straight Arrhenius plot over ten orders of magnitude [19, 20] despite the fact that Schober's model exhibits the most pronounced temperature dependence for H^m of all [15]. Although one can assume [15, 14] that the formation enthalpy is also affected by strongly temperature-dependent phonon modes, making this assumption is probably not really justified, if one considers that the energy necessary to form a vacancy is primarily due to the change in energy of the free electrons. In this context, it is not unreasonable to assume the vacancy formation enthalpy to change with temperature when the elastic force constants change nonlinearly with temperature; yet an estimation of the order of magnitude by Flynn [35] shows that the change in elastic force constants affects the formation enthalpy only to a third of the fractional extent to which the migration enthalpy is changed.

In summary, it is obvious that although considerable progress has been achieved in recent years by calculating vacancy migration enthalpies and their temperature dependence on the basis of phonon dispersion data, the theoretical verification of curved Arrhenius plots of the self-diffusion in bcc metals has still not been achieved in a quantitative manner. The discussion has shown that our conclusions concerning the experimental results are not unambiguous, since the vacancy migration enthalpy H^m has not yet been calculated for pure β-Hf for various temperatures and the alloying effects of group IV–V metals are not understood in full detail. Despite the above-discussed experiments, it is not unlikely that the experimental results presented here give a further indication that the concept of a monovacancy model with temperature-dependent activation energies still needs some clarification.

5. Summary

Measurements of the tracer diffusion of ^{181}Hf, ^{95}Nb and ^{95}Zr in a Hf–Nb(10 at.%) and Hf–Nb(18 at.%) alloy yielded *linear* Arrhenius relations. The random alloy model of Manning was applied, yielding values of 0.728–0.731 for the correlation factor of Hf self-diffusion, indicating that the dominant diffusion mechanism in β-Hf is the monovacancy mechanism. The experimental results were discussed on the basis of the model of a phonon-related diffusion process. Whether the results can be explained within this model remains questionable.

Acknowledgments

We are indebted to J Trampenau for providing experimental results on phonon dispersion measurements in the Zr–Nb system before publication. This work was supported by the German Bundesministerium für Forschung und Technologie under contract No 03-HE3MUE.

References

[1] Mehrer H, Stolica N and Stolwijk N A 1990 *Landolt–Börnstein New Series* Group III, vol 26 (Berlin: Springer) p 32
[2] Herzig C and Köhler U 1988 *Mater. Sci. Forum* **15–18** 301
[3] Seeger A and Mehrer H 1970 *Vacancies and Interstitials in Metals* ed A Seeger, D Schumacher, W Schilling and J Diehl (Amsterdam: North-Holland) p 1
[4] Siegel R W 1983 *Point Defects and Defect Interactions* (Tokyo: University of Tokyo Press) p 533
[5] Seeger A 1993 *Defect Diffusion Forum* **95–98** p 147
[6] Varotsos P A, Ludwig W and Alexopoulos K D 1978 *Phys. Rev.* B **18** 2683
[7] Gilder H M and Lazarus D 1975 *Phys. Rev.* B **11** 4916
[8] Köhler U and Herzig C 1988 *Phil. Mag.* A **58** 769
[9] Petry W, Heiming A, Herzig C and Trampenau J 1991 *Defect Diffusion Forum* **75** 157
[10] Petry W, Heiming A, Trampenau J, Alba M, Herzig C, Schober H R and Vogl G 1991 *Phys. Rev.* B **43** 10933
[11] Heiming A, Petry W, Trampenau J, Alba M, Herzig C, Schober, H R and Vogl G 1991 *Phys. Rev.* B **43** 10948
[12] Trampenau J, Heiming A, Petry W, Alba M, Herzig C, Miekeley W and Schober H R 1991 *Phys. Rev.* B **43** 10963
[13] Trampenau J, Petry W and Herzig C 1993 *Phys. Rev.* B **47** 3132
[14] Güthoff F, Hennion B, Herzig C, Petry W, Schober H R and Trampenau J 1994 *J. Phys.: Condens. Matter* **6** 6211
[15] Schober H R, Petry W and Trampenau J 1992 *J. Phys.: Condens. Matter* **4** 9321
[16] Vogl G, Petry W, Flottmann T and Heiming A 1989 *Phys. Rev.* B **39** 5025
[17] Herzig C and Eckseler H 1979 *Z. Metallk.* **70** 215
[18] Maier K, Mehrer H and Rein G 1979 *Z. Metallk.* **70** 209
[19] Mundy J N, Tse C W and McFall W D 1976 *Phys. Rev.* B **13**
[20] Mundy J N, Hoff H A, Pelleg J, Rothman S J, Nowicki L J and Schmidt F A 1981 *Phys. Rev.* B **24**
[21] Bußmann W, Herzig C, Hoff H A and Mundy J N 1981 *Phys. Rev.* B **23** 6216
[22] Herzig C and Bußmann G 1982 *Point Defects and Defect Interactions in Metals* (Tokyo: University of Tokyo Press) p 578
[23] Köhler U and Herzig C 1987 *Phys. Status Solidi* b **144** 243
[24] Massalski T B, Murray J L, Bennet L H, Baker H and Kacprzak L 1986 *Binary Alloy Phase Diagrams* (Metals Park, OH: American Society of Metals)
[25] Büscher M 1992 *PhD Thesis*, Universität Münster
[26] Manning J R 1967 *Acta Metall.* **15** 817
[27] Manning J R 1968 *Diffusion Kinetics for Atoms in Crystals* (Princeton, NJ: Van Nostrand Reinhold)

[28] Itayama N and Stüwe H P 1974 *Z. Metallk.* **65** 70
[29] Mundy J N, Ockers S T and Smedskjaer L C 1986 *Phys. Rev.* B **33** 847
[30] Herzig C and Köhler U 1987 *Acta Metall.* **35** 7
[31] Petry W, Heiming A, Trampenau J and Vogl G 1989 *Defect Diffusion Forum* **66–69** 157
[32] DeFontaine D and Buck O 1973 *Phil. Mag.* **27** 967
[33] Trampenau J 1991 *PhD Thesis* Universität Münster
[34] Herzig C, Köhler U and Büscher M 1993 *Defect Diffusion Forum* **95–98** 793
[35] Flynn C P 1968 *Phys. Rev.* **171** 682